



Article

An Improved Method for Estimating Sea Surface Temperature Based on GF-5A Satellite Data in Bohai Bay

Jiren Sun ¹, Daoming Wei ², Dianjun Zhang ^{1,*} and Zhiwei Sun ³

- School of Marine Science and Technology, Tianjin University, Tianjin 300072, China; 3018001187@tju.edu.cn
- ² Key Laboratory of Smart Earth, Beijing 100029, China; 13716430611@163.com
- ³ Beijing Geoway Info-Tech Co., Ltd., Beijing 100043, China; 176117@tju.edu.cn
- * Correspondence: zhangdianjun@tju.edu.cn; Tel.: +86-022-85350655

Abstract: Sea surface temperature (SST) is an important physical parameter that plays an important role in the study of various dynamic and thermodynamic processes in the ocean. Common SST retrieval methods are divided into single-channel methods (such as the single window algorithm) and multi-channel methods (such as the split window algorithm). To solve the problem of the low resolution of SST data used in coastal research, this study proposed a split window algorithm by adjusting the two important parameters, atmospheric transmittance and regression coefficients, to estimate SST using remotely sensed GF-5A images with a resolution of 100 m. The results were indirectly validated using MODIS temperature product and directly validated using measured data. The GF-5A image data obtained on 18 July 2024 were compared with MODIS data, giving R^2 of 0.985 and RMSE of 0.139 K. For the GF-5A image data obtained on 31 December 2024, the indirectly verified R^2 was 0.996 and the RMSE was 0.116 K. The R^2 and RMSE values of the direct verification of the accuracy of data from the two GF-5A images and the measured data were 0.999 and 0.613 K, respectively, which are better than the SST retrieval results of Landsat 8 data obtained at the same resolution. This work provides data support for subsequent research on the ecological environment and plant resources in the Bohai Bay.

Keywords: GF-5A; sea surface temperature (SST); split window algorithm; Bohai Bay



Academic Editor: Yukiharu Hisaki

Received: 15 March 2025 Revised: 25 May 2025 Accepted: 26 May 2025 Published: 28 May 2025

Citation: Sun, J.; Wei, D.; Zhang, D.; Sun, Z. An Improved Method for Estimating Sea Surface Temperature Based on GF-5A Satellite Data in Bohai Bay. *Remote Sens.* **2025**, *17*, 1879. https://doi.org/10.3390/rs17111879

Copyright: © 2025 by the authors. Licensee MDPI, Basel, Switzerland. This article is an open access article distributed under the terms and conditions of the Creative Commons Attribution (CC BY) license (https://creativecommons.org/licenses/by/4.0/).

1. Introduction

As an important physical parameter, SST plays an important role in marine research fields such as marine pollution prevention, fishery resources protection and development, and dynamic monitoring of marine ecological environments. Due to the recent increase in the frequency of abnormal climate phenomena such as El Niño, it is crucial to study SST, which is closely associated with these abnormal climate phenomena [1].

The traditional method of obtaining SST has high accuracy and uses various discrete observation points, such as buoys and shipborne sensors, however, it is difficult to represent the large-scale ocean state. Satellite remote sensing technology, which is superior to the traditional methods, can enable synchronous acquisition of large-scale spatio-temporal SST data. The commonly used SST retrieval algorithms are divided into single-channel retrieval algorithms, which use one thermal infrared data channel [2], and multi-channel retrieval algorithms, which use multiple thermal infrared data channels [3].

The single channel method is mainly divided into the radiative transfer equation method [4], the mono-window algorithm [5–7], and the generalized single-channel method [8–10]. Although the single-channel SST retrieval method has been used for many years, it still has many problems. The radiative transfer equation method needs accurate

Remote Sens. 2025, 17, 1879 2 of 16

real-time atmospheric profile parameter data to have high accuracy in temperature retrieval, and it is difficult to obtain accurate real-time atmospheric profile parameter data for use in practical applications [11]. In the mono-window algorithm, the atmospheric profile data simulation still requires some parameter estimation, which makes the applicability of the single-window algorithm low [12]. The empirical formula in the universal single-channel method is not universal. When the atmospheric water vapor content is high, the empirical formula fails and generates large errors [13]. The multi-channel temperature inversion algorithm eliminates the atmospheric effect through differences in the atmospheric effect in different thermal infrared bands. Therefore, the temperature retrieval algorithm for atmospheric correction can be realized by using satellite data, which reduces the demand for atmospheric parameters [14,15]. The Qin split window algorithm has the advantages of fewer input parameters, a simple calculation process, strong applicability, and high temperature inversion accuracy [16]. In conclusion, compared with single-channel algorithms, the Qin split window algorithm can achieve higher in SST retrieval accuracy with fewer atmospheric parameters, making it a reliable SST retrieval method [17–19].

However, in recent years, people have used the split window algorithm for the retrieval of satellite-based temperature data at different resolutions, for example, the Visible-Infrared Spin Scan Radiometer (VISSR) data from the FY-2C satellite with a 5-km resolution [20], the INSAT imager data from the INSAT-3D satellite with a 4-km resolution [21], the Spinning Enhanced Visible and Infrared Imager (SEVIRI) data from the MSG satellite at a 3-km resolution [22,23], the Advanced Himawari Imager (AHI) data from the Himawari 8 satellite with a 2-km resolution [24], the Visible and Infrared Radiometer (VIRR) data from the FY-3A satellite with a 1.1-km resolution [25], the Advance Very High Resolution Radiometer (AVHRR) data from the NOAA satellite with a 1.1-km resolution [26], the Moderate-Resolution Imaging Spectroradiometer (MODIS) data from the Earth Observation System (EOS) TERRA/AQUA satellite with a 1-km resolution [27], the Sea and Land Surface Temperature Radiometer (SLSTR) data from the Sentinel-3 satellite with a 1-km resolution [28], the wide-band imager data from the Tiangong-2 satellite with a 400-m resolution [29], and the Medium Resolution Spectral Imager -2 (MERSI-2) data from the FY-3D satellite with a 250-m resolution [30]. However, the resolutions of these satellite data are still too low for coastal research. Given the low resolution of the satellite used in split window algorithm temperature data retrieval, this paper uses the Wide-swath Thermal Infrared Imager (WTI) data from the GF-5A satellite with a 100-m resolution and modifies the parameters used in the Qin split window algorithm according to GF-5A satellite parameters to achieve high-precision SST data retrieval for the Bohai Bay area.

2. Study Area and Data

2.1. Study Area

The area analyzed in this study is Bohai Bay, one of the three major bays in China's Bohai Sea. As Figure 1, its latitude and longitude range is 38°1′N–39°13′N, 117°34′E–119°5′E. Bohai Bay is surrounded by land on three sides, with the northern part being a famous tourist and resort area, and Tanggu in the west being an important port. It is also the maritime gateway to Beijing–Tianjin–Hebei, and the hub of North China shipping [31].

Retrieval of SST data for the Bohai Bay facilitates the study of the growth of zoo-plankton and phytoplankton communities [32,33], the temporal and spatial distribution characteristics of fish eggs [34], the temporal and spatial changes in regional thermal structure [35], and the protection and sustainable development of the ecological environment [36].

Remote Sens. 2025, 17, 1879 3 of 16

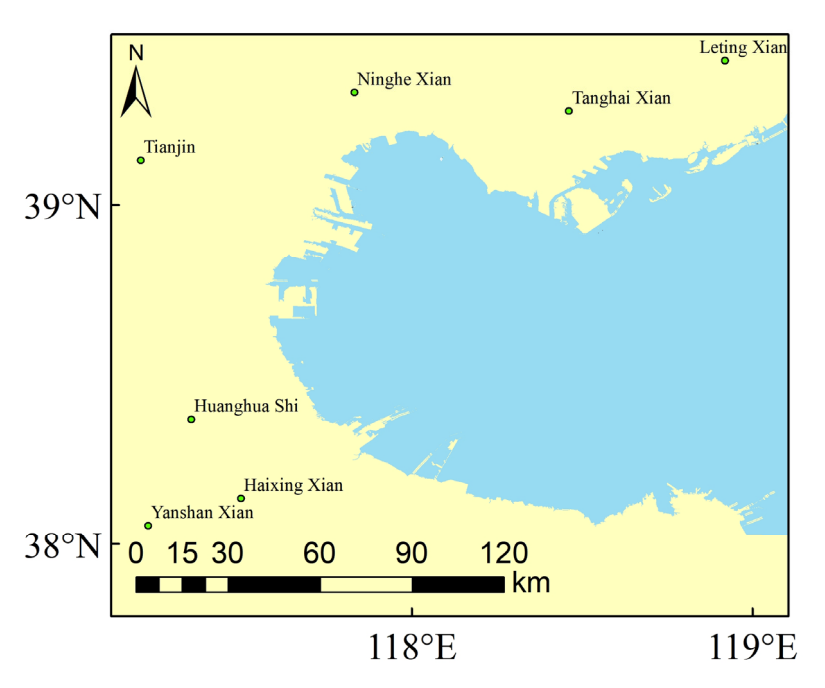


Figure 1. Schematic diagram of Bohai Bay.

2.2. Data

2.2.1. Measured Data

The data were obtained from the global marine data of National Centers for Environmental Information (https://www.ncei.noaa.gov/maps/marine/, accessed on 20 April 2024). The measured data are scattered data obtained through observations from ships, buoys, and other platforms. This study obtained measured data covering a period similar to two GF-5A images for direct verification of SST retrieval accuracy. The specific measured data are shown in Table 1.

Table 1. Specific measured data.

Station	Time	Longitude	Latitude
ZCPC7MW	27 December 2024 07:00	118.6°E	38.8°N
KUL7SEK	29 December 2024 03:00	$118.7^{\circ}\mathrm{E}$	38.8°N
CQNL	28 December 2024 12:00	118.8°E	38.8°N
SJGS5AE	5 January 2025 18:00	119.1°E	38.7°N
KKEKFPK	23 July 2024 17:00	118.3°E	38.9°N
KKEKFPK	23 July 2024 18:00	118.2°E	38.9°N
KKEKFPK	23 July 2024 19:00	118.1°E	38.9°N
KKEKFPK	25 July 2024 05:00	118.0°E	38.9°N
KKEKFPK	25 July 2024 06:00	118.2°E	38.9°N
KKEKFPK	25 July 2024 09:00	118.9°E	38.8°N
KKEKFPK	25 July 2024 10:00	119.1°E	38.7°N

2.2.2. MODIS

These data were obtained from LADDS DAAC (https://ladsweb.modaps.eosdis.nasa.gov). MODIS is an important instrument carried on the EOS TERRA/AQUA satellites. The Terra and Aqua satellites are part of the EOS program and can simultaneously collect information about Earth's atmosphere, land, oceans, and solar energy balance. EOS takes the Earth as a whole and studies the Earth's system comprehensively through Earth system science and space technology, thus contributing to the study of the Earth's system and global environmental changes. MODIS has a resolution of 1 km and is used to observe global biological and physical processes. MODIS has 36 discrete spectral stages, with a

Remote Sens. 2025, 17, 1879 4 of 16

wide spectral range from $0.4~\mu m$ to $14.4~\mu m$, and provides information on various important physical quantities. The MODIS data used in this study are shown in Table 2 [37,38].

Table 2. MODIS data used in this study.

Name	Name Information	
MOD03	MODIS geolocation data file, which contains the longitude and latitude of each 1 km Earth view center	Geometric correction for remote sensing image
MOD021KM	MODIS1B data product with a resolution of 1km; include reflectance and emissivity datasets	The reflectivity of band 2 and band 19 are used to calculate the atmospheric water vapor content
MODIS temperature product	MODIS temperature product with a resolution of 1 km	Used for indirect verification of SST retrieval results

2.2.3. GF-5A

The GF-5A satellite is also known as the hyperspectral comprehensive observation satellite. It has three loads: Environmental trace gases Monitoring Instrument (EMI), the Advanced Hyperspectral Imager (AHSI), and WTI. EMI is used to measure the Earth's backscattered radiation in the ultraviolet and visible spectral range to facilitate the detection of atmospheric trace gases. AHSI is used for ground object detection and recognition through hyperspectral resolution imaging with wide coverage and spectral bands. WTI provides a wide range of day and night thermal infrared images for SST retrieval. It has the comprehensive detection ability of all day, multi-element. It provides key data support for many studies, such as ecological environment protection, natural resource monitoring, and climate change research. GF-5A's WTI parameters are presented in Table 3.

Table 3. The GF-5A satellite's WTI parameters.

Parameter	Parameter Value	
Spectral segment	B1: 8.01–8.39 μm B2: 8.42–8.83 μm B3: 10.3–11.3 μm B4: 11.5–12.5 μm	
Sub-satellite ground pixel resolution	≤100 m	
Width	≥1500 km	

2.2.4. Landsat 8-9 C2L2

The data were obtained from USGS (https://www.usgs.gov/). Landsat series satellites are the main systems for medium-resolution remote sensing in the Earth observation system of the United States. They play an important role in the investigation and management of land and marine resources. The Landsat 8-9 satellite is the fourth generation product, and its C2L2 data are the atmospheric corrected surface reflectance data, which are suitable for a variety of remote sensing applications. In this study, QA_PIXEL band data were used for cloud removal and sea–land separation. The QA_PIXEL band is used for pixel quality assessment, and the specific meanings of its values are presented in Table 4.

Remote Sens. 2025, 17, 1879 5 of 16

Table 4. The meanings of different binary values of the QA_PIXEL band data.

Bit	Flag Description	Value
0	Fill	0 image data 1 fill data
1	Dilated Cloud	0 cloud is not dilated or no cloud 1 cloud dilation
2	Cirrus	0 cirrus confidence: no confidence level set for low confidence 1 high confidence
3	Cloud	0 cloud confidence is not high 1 high confidence
4	Cloud Shadow	0 cloud shadow confidence is not high 1 high confidence
5	Snow	0 snow/ice confidence is not high 1 high confidence
6	Clear	0 cloud or dilated cloud bits are set 1 cloud and dilated cloud bits are not set
7	Water	0 land or cloud 1 water
8–9	Cloud Confidence	00 no confidence level set 01 low confidence 10 medium confidence 11 high confidence
10–11	Cloud Shadow Confidence	00 no confidence level set 01 low confidence 10 reserved 11 high confidence
12–13	Snow/Ice Confidence	00 no confidence level set 01 low confidence 10 reserved 11 high confidence
14–15	Cirrus Confidence	00 no confidence level set 01 low confidence 10 reserved 11 high confidence

3. Methods

3.1. GF-5A Data Preprocessing

Because MODIS, Landsat, and GF-5A data have different resolutions, it is necessary to resample MODIS and Landsat data so that their resolutions are consistent with those of GF-5A data.

The original GF-5A satellite thermal infrared band data need to be preprocessed. Figure 2 shows the preprocessing process of GF-5A satellite data. GF-5A has four thermal infrared bands. Based on the application of the split window algorithm, band 3 and band 4 are the most suitable for SST retrieval using the split window algorithm [39]. First, the clouds are removed and sea and land are separated in the GF-5A satellite data using Landsat 8–9 C2L2 QA_PIXEL band data. Then, the radiances of band 3 and band 4 are obtained via radiometric correction based on the coefficients in the metadata file. Finally, the brightness temperatures of band 3 and band 4 are obtained by substituting the effective wavelength and radiance into the formula.

Remote Sens. 2025, 17, 1879 6 of 16

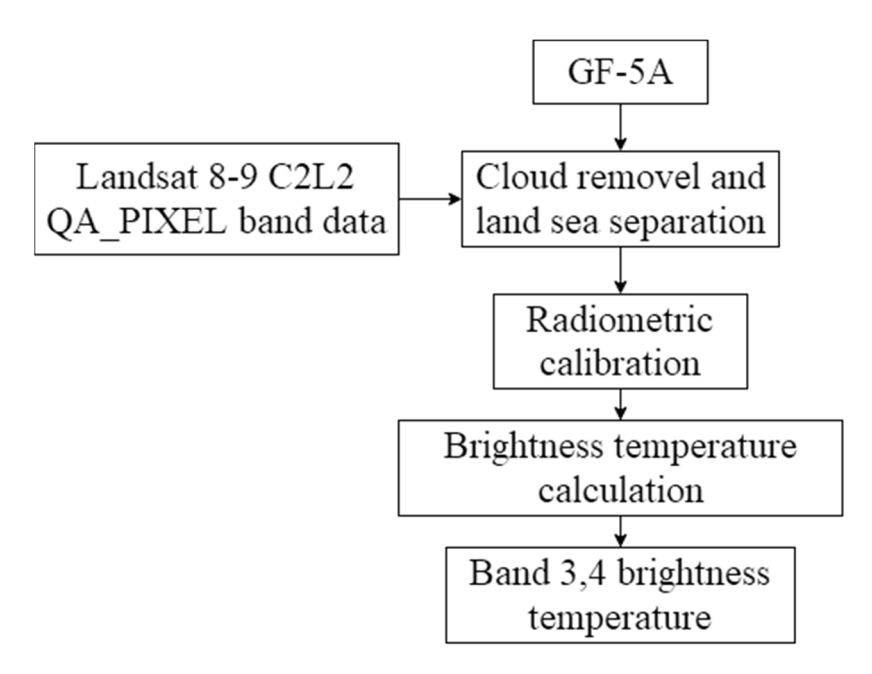


Figure 2. GF-5A satellite data preprocessing process.

Radiometric calibration is the process of converting the digital quantization value (DN) of GF-5A satellite images into physical quantities such as radiance, reflectivity, or surface temperature values. Radiometric calibration parameters can be obtained from the metadata file of the GF-5A satellite.

$$B = A_0 + A_1 \times DN + A_2 \times DN^2 \tag{1}$$

Equation (1) represents the radiometric calibration formula, where B is the radiance; DN is the digital quantization value; and A_0 , $A_{1,}$ and A_2 are the radiation calibration parameters in the metadata files.

If the spectral radiation intensity of an actual object is equal to that of a blackbody at the same wavelength, the temperature of the blackbody at that time is called the brightness temperature of the actual object at that wavelength. Brightness temperature is an important parameter in the retrieval of SST data. Calculation of brightness temperature requires the effective wavelength of the thermal infrared band, and the calculation of effective wavelength requires the spectral response function of the thermal infrared band.

Spectral response function refers to the ratio of received radiance to incident radiance at each wavelength of the sensor and describes the response intensity of a sensor at different wavelengths. The spectral response function of the GF-5A satellite's wide-range thermal infrared imager was queried through the China Centre for Resources Satellite Data and Application. Figure 3 shows the spectral response function of the GF-5A satellite's wide-range thermal infrared imager.

$$\lambda_e = \frac{\int_{\lambda_{min}}^{\lambda_{max}} f(\lambda) \lambda d\lambda}{\int_{\lambda_{min}}^{\lambda_{max}} f(\lambda) d\lambda}$$
 (2)

Equation (2) represents the effective wavelength calculation formula, where $f(\lambda)$ is the spectral response function, λe is the effective wavelength, and λ is the wavelength.

$$T = \frac{hc}{\lambda_e k ln \left(1 + \frac{2hc^2}{\lambda_o^2 B}\right)} \tag{3}$$

Remote Sens. 2025, 17, 1879 7 of 16

Equation (3) represents the inverse of the Planck function, where T is the brightness temperature, c is the speed of light, h is the Planck constant, k is the Boltzmann constant, and B is the radiance.

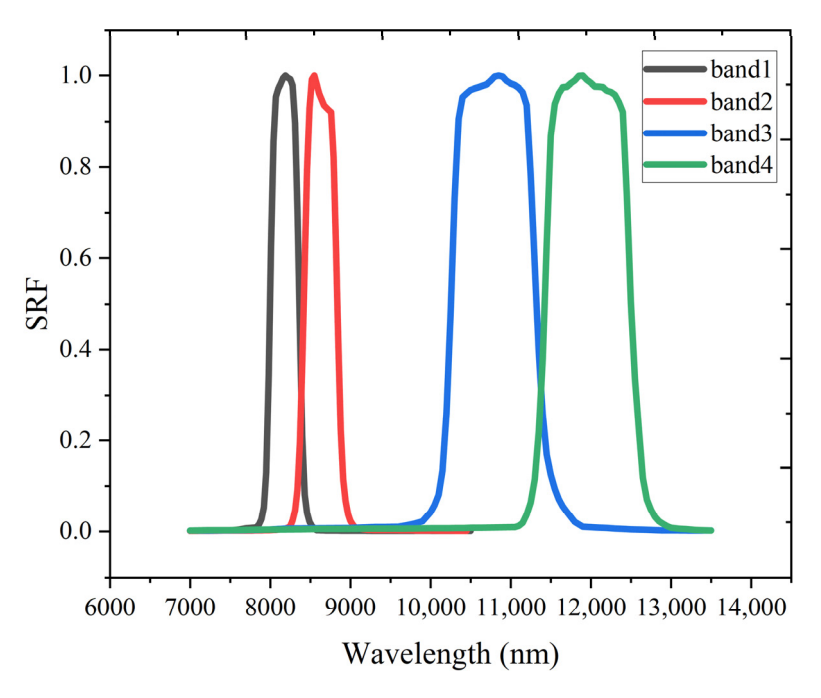


Figure 3. Spectral response function of the GF-5A satellite's wide-range thermal infrared imager.

3.2. Qin Split Window Algorithm for GF-5A Satellite Data

The SST retrieval in this study first corrected the two important parameters, atmospheric transmittance and regression coefficient, based on the band 3 and band 4 parameters of the GF-5A satellite, and then combined the brightness temperatures of band 3 and band 4 to obtain SST using the Qin split window algorithm. Finally, the retrieved SST results were verified indirectly using MODIS temperature product and directly using measured data. Figure 4 shows the process of retrieving SST.

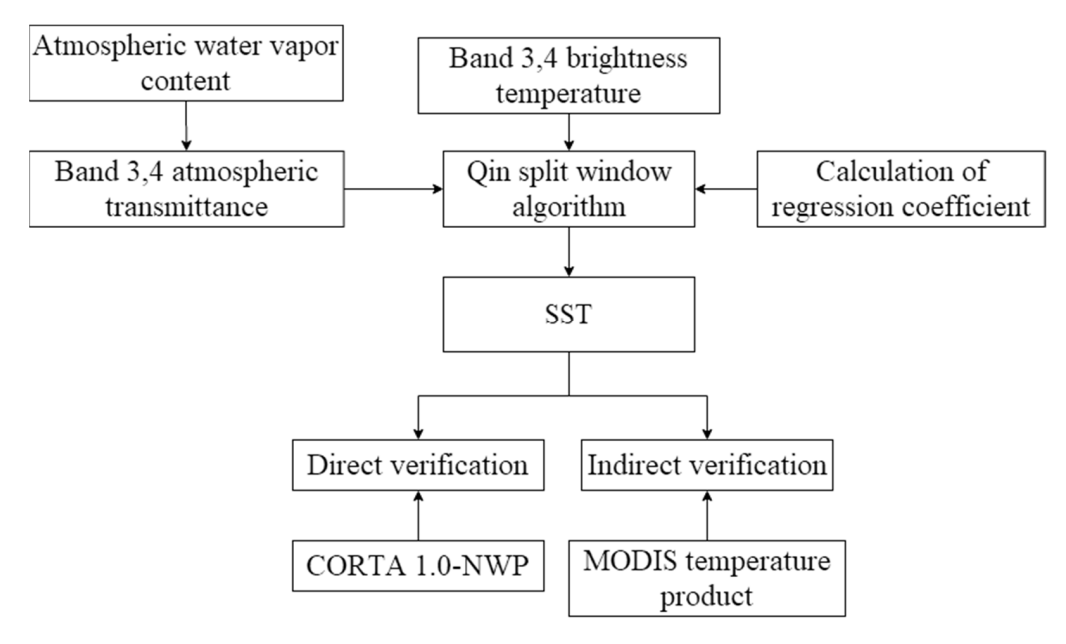


Figure 4. SST data retrieval process.

Remote Sens. 2025, 17, 1879 8 of 16

3.2.1. Adjustment of Atmospheric Transmittance

Atmospheric water vapor content is an important parameter affecting atmospheric transmittance, which is calculated from the reflectivity of band 2 and band 19 in MOD021km.

$$\omega = \left(\frac{\left(\alpha - \ln \frac{R_{19}}{R_2}\right)}{\beta}\right)^2 \tag{4}$$

Equation (4) represents the formula for calculating atmospheric water vapor content, where ω is the atmospheric water vapor content, R_{19} is the reflectivity of MOD021km band 19, R_2 is the reflectivity of MOD021km band 2, $\alpha = 0.02$, and $\beta = 0.651$.

Atmospheric transmittance is the ratio of the electromagnetic radiation flux after atmospheric attenuation to the electromagnetic radiation flux at the point when electromagnetic waves propagate in the atmosphere. It is an important parameter that affects the retrieval results of SST, and its calculation needs to be adjusted according to the parameters of different satellites.

In this study, Ψ_1 was calculated using the effective wavelength. The atmospheric transmittance formula suitable for GF-5A satellite data was obtained as follows.

$$\tau = \frac{1}{\Psi_1} = \frac{1}{a\omega^3 + b\omega^2 + c\omega + d} \tag{5}$$

Equation (5) represents the formula for calculating atmospheric transmittance [8], where τ is the atmospheric transmittance, ω is the atmospheric water vapor content, and a, b, c, and d are the effective wavelength functions.

Because the brightness temperature and satellite zenith angle also affect atmospheric transmittance, and the effective wavelengths of band 3 and band 4 of the GF-5A satellite are close to those of MODIS band 31 and band 32, the angle correction value and temperature correction value for atmospheric transmittance are introduced [40].

$$\tau_3(\theta) = -0.00247 + (2.3652 \times 10^{-5})\theta^2
\tau_4(\theta) = -0.00322 + (3.0967 \times 10^{-5})\theta^2$$
(6)

Equation (6) represents the formula for calculating the atmospheric transmittance angle correction value, and θ is the sensor zenith angle.

$$\tau_{3}(T) = \begin{cases}
0.08; T_{3} \ge 298.15 \\
-0.05 + 0.00325(T_{3} - 5); 278.15 < T_{3} < 298.15 \\
-0.05; T_{3} \le 278.15
\end{cases}$$

$$\tau_{4}(T) = \begin{cases}
0.095; T_{4} \ge 298.15 \\
-0.065 + 0.004(T_{4} - 5); 278.15 < T_{4} < 298.15 \\
-0.065; T_{4} \le 278.15
\end{cases}$$
(7)

Equation (7) represents the formula for calculating the atmospheric transmittance temperature correction value. T_3 and T_4 are the brightness temperatures for band 3 and band 4 of the GF-5A satellite.

3.2.2. Adjustment of Regression Coefficients

Regression coefficients a and b are also important parameters that affect the retrieval results of SST, and their calculation also needs to be adjusted for different satellites. The Planck formula is expanded linearly based on the Taylor series, and the temperature

Remote Sens. 2025, 17, 1879 9 of 16

parameter L can be defined. Its value has a good linear relationship with the brightness temperature T.

$$L = a + bT = \frac{B}{\frac{\partial B}{\partial T}} \tag{8}$$

Equation (8) is the regression coefficient calculation formula, where a and b are the regression coefficients, B is the radiance, and T is the brightness temperature.

3.2.3. SST Data Retrieval

The brightness temperatures of band 3 and band 4 of GF-5A images, together with the atmospheric transmittance and regression coefficient corrected above, are imported into the formula of the Qin split window algorithm to enable SST retrieval.

$$SST = A_0 + A_1 T_3 - A_2 T_4$$

$$A_0 = \frac{a_3 D_4 (1 - C_3 - D_3) - a_4 D_3 (1 - C_4 - D_4)}{D_4 C_3 - D_3 C_4}$$

$$A_1 = 1 + \frac{D_3 + b_3 D_4 (1 - C_3 - D_3)}{D_4 C_3 - D_3 C_4}$$

$$A_2 = \frac{D_3 [1 + b_4 (1 - C_4 - D_4)]}{D_4 C_3 - D_3 C_4}$$

$$C_3 = \mathcal{E} \tau_3; C_4 = \mathcal{E} \tau_4; D_3 = (1 - \tau_3) [1 + (1 - \mathcal{E}) \tau_3]; D_4 = (1 - \tau_4) [1 + (1 - \mathcal{E}) \tau_4]$$

Equation (9) is the formula for calculating the Qin split window algorithm, where ε is the surface specific emissivity, and the value of water body is usually 0.995 [41]; T_3 and T_4 are the brightness temperatures of the GF-5A satellite's band 3 and band 4; τ_3 and τ_4 are the atmospheric transmittance values of the GF-5A satellite's band 3 and band 4, C and D are intermediate parameters of GF-5A satellite's band 3 and band 4, which are calculated using ε , τ_3 , and τ_4 ; a_3 , b_3 , a_4 , and b_4 are the regression coefficients of GF-5A satellite's band 3 and band 4.

3.3. Accuracy Verification Index Value

 R^2 is the determination coefficient, and is used to measure the linear relationship between SST retrieval results and validation data at the same pixel scale. The value range is [0,1]. A value closer to 1 indicates that the overall deviation between SST retrieval results and validation data is small, and the retrieval accuracy is high.

$$R^{2} = 1 - \frac{\sum_{i=1}^{n} (y_{i} - \hat{y}_{i})^{2}}{\sum_{i=1}^{n} (y_{i} - \overline{y})^{2}}$$
(10)

Equation (10) is the formula for calculating R^2 , where R^2 is the determination coefficient, n is the number of selected points, y_i is the SST retrieval result value, \overline{y} is the average value of SST retrieval results, and $\hat{y_i}$ is the validated data value.

RMSE is the root mean square error or standard error, and can reflect the deviation between SST results and validation data. The lower the value, the higher the accuracy of the SST result retrieval.

$$RMSE = \sqrt{\frac{1}{n} \sum_{i=1}^{n} (y_i - \hat{y}_i)^2}$$
 (11)

Equation (11) is the formula for calculating *RMSE*, where *RMSE* is the root mean square error or standard error, n is the number of selected points, y_i is the SST result retrieval value, and $\hat{y_i}$ is the validated data value.

4. Results

4.1. Determination of Atmospheric Transmittance

Atmospheric transmittance is the ratio of the electromagnetic radiation flux after atmospheric attenuation when electromagnetic waves propagate into the atmosphere to when the electromagnetic radiation flux is incident on the surface. It has a great influence on the transmission of thermal radiation and is significantly affected by the atmospheric water vapor content.

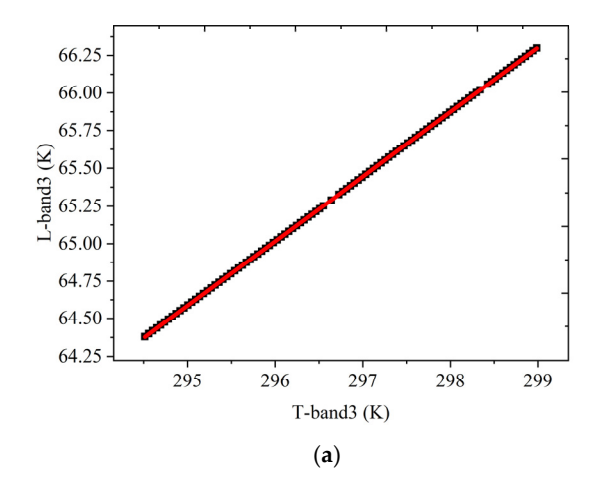
The atmospheric transmittance correction in this study was calculated using the effective wavelength and atmospheric water vapor content. The effective wavelength is calculated using the band response function in Equation (2), and then substituted into the formula for calculating the four coefficients a, b, c, and d in Equation (5). The formula and results are shown in Table 5. The atmospheric water vapor content is calculated using Equation (4), and the corrected atmospheric transmittance is obtained by substituting this into Equation (5) and adding the angle and temperature correction values.

Table 5. Formu	lae and result	s of four co	efficients (a,	b, c , and d).

Name	Calculation Formula	Band 3 Results	Band 4 Results
a	$0.0009\lambda e^3 - 0.01638\lambda e^2 + 0.04745\lambda e + 0.27436$	0.01	0.0384
b	$0.00032\lambda e^3 - 0.06148\lambda e^2 + 1.2021\lambda e - 6.2051$	0.0097	-0.0742
c	$0.00986\lambda e^3 - 0.23672\lambda e^2 + 1.7133\lambda e - 3.2199$	0.0933	0.2775
d	$-0.15431\lambda e^3 + 5.2757\lambda e^2 - 60.117\lambda e + 229.3139$	1.0224	0.9696

4.2. Determination of Regression Coefficients

Based on Equations (1)–(3) and (8), the values of regression coefficients a and b are only associated with the effective wavelength and radiometric calibration coefficient. Therefore, the thermal infrared bands of different satellites have different effective wavelengths, and different satellite remote sensing images have different radiometric calibration coefficients, leading to different regression coefficient values for a and b. The fitting curves of temperature parameter b and brightness temperature b of band 3 and band 4 of the two remote sensing images in this study are shown in Figures 5 and 6. The results are completely linear, and the regression coefficients b and b can be obtained using Equation (8); the results are shown in Table 6.



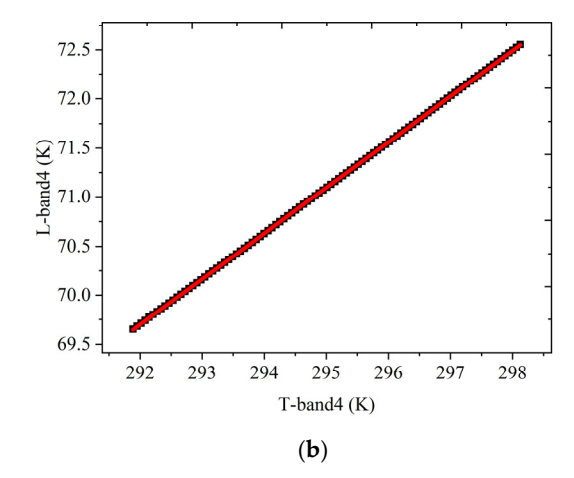
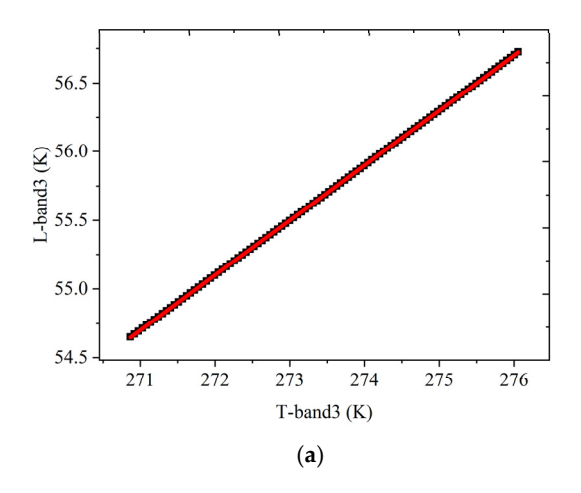


Figure 5. The relationship between temperature parameter *L* and brightness temperature *T* in bands 3 and 4 of the 18 July 2024 GF-5A satellite image. (a) Band 3; (b) band 4.



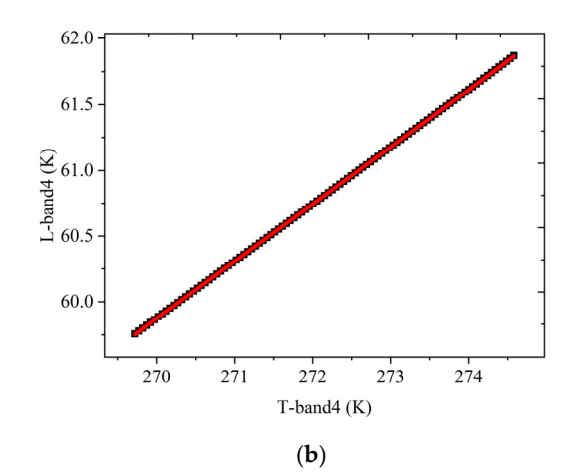


Figure 6. The relationship between temperature parameter *L* and brightness temperature *T* in bands 3 and 4 of the 31 December 2024 GF-5A satellite image. (a) Band 3; (b) band 4.

Table 6. Regression coefficients of bands 3 and 4 in two GF-5A satellite images obtained on 18 July 2024 and 31 December 2024.

		Regression Coefficient a	Regression Coefficient b
18 July 2024	Band 3	-62.00847	0.42913
	Band 4	-66.10467	0.46508
31 December 2024	Band 3	-53.5938	0.39961
	Band 4	-57.53953	0.43487

4.3. SST Retrieval Results

Two GF-5A remote sensing images were used to retrieve SST data based on the Qin split window algorithm using the corrected atmospheric transmittance, regression coefficients, and band 3 and band 4 data. Comparisons of the SST retrieval results of two GF-5A images and MODIS temperature product are shown in Figures 7 and 8.

The results show that SST in the Bohai Bay area decreased gradually from the shore to the sea from 18 July 2024, and then increased gradually from the shore to the sea from 31 December 2024. The SST range in the Bohai Bay area was 26–30 $^{\circ}$ C from 18 July 2024 and 1–7 $^{\circ}$ C from 31 December 2024. Figures 7 and 8 show that the SST results retrieved in this study have the same spatial distribution as the MODIS temperature products.

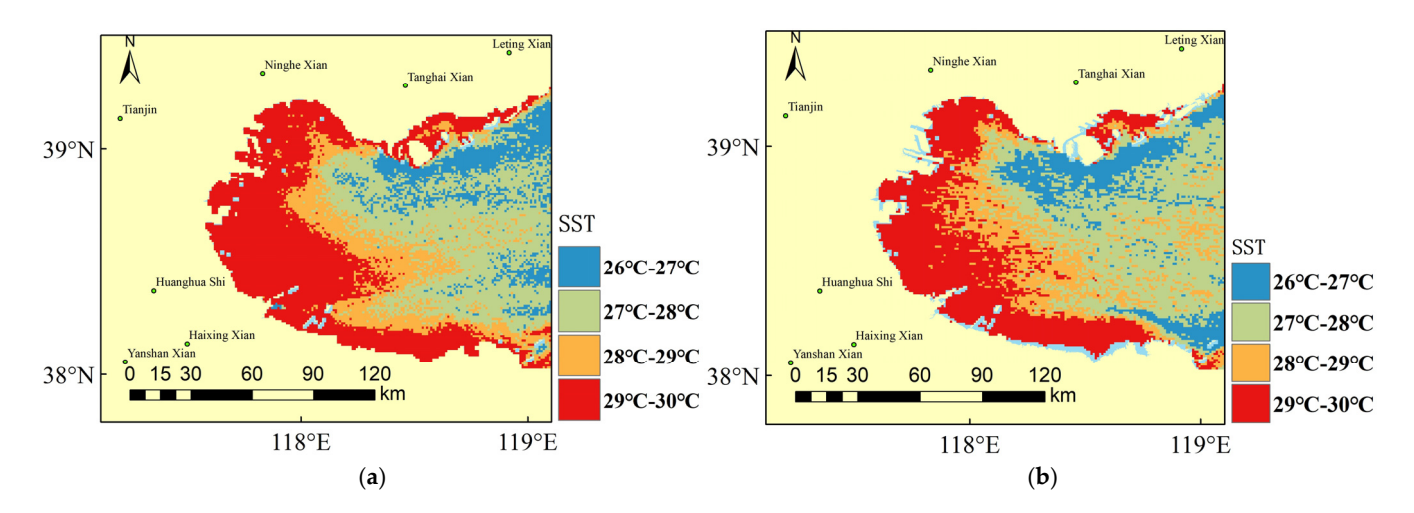


Figure 7. Comparison of SST retrieval results of GF-5A and resampled MODIS temperature product images obtained on 18 July 2024. (a) GF-5A; (b) MODIS temperature product.

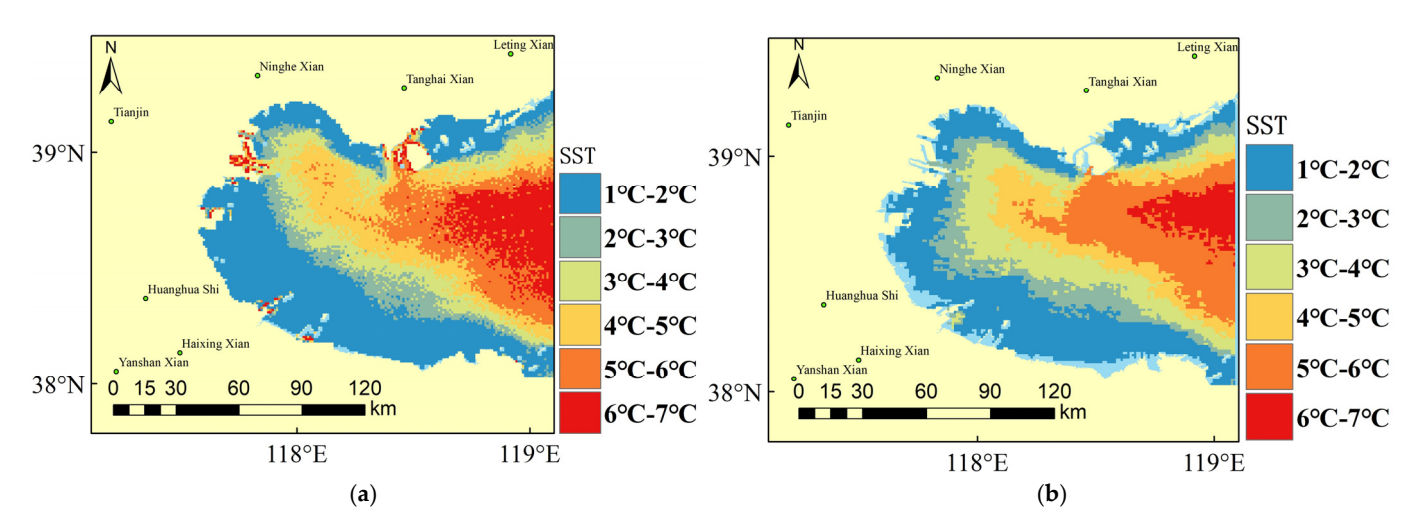


Figure 8. Comparison of SST retrieval results of GF-5A and resampled MODIS temperature product images obtained on 31 December 2024. (a) GF-5A; (b) MODIS temperature product.

4.4. Validation of Retrieved SST Results

The retrieved SST results were compared with the SST results obtained from MODIS temperature product to indirectly verify the accuracy of SST results retrieval. The retrieved SST results were compared with the measured SST data to directly verify the accuracy of SST results retrieval. The indirect verification of the accuracy of SST results retrieval in this study is shown in Figure 9, and the direct verification of the accuracy of the results retrieval is shown in Figure 10. The results of the analysis of the error between the indirect and direct verification of the accuracy of SST results retrieval are shown in Table 7.

Table 7. Analysis of the accuracy of SST results retrieval from two GF-5A satellite remote sensing images.

	Indirect Verification		Direct Verification
	18 July 2024	24 31 December 2024 Direct V	
R^2	0.985	0.996	0.999
RMSE	0.139 K	0.116 K	0.613 K

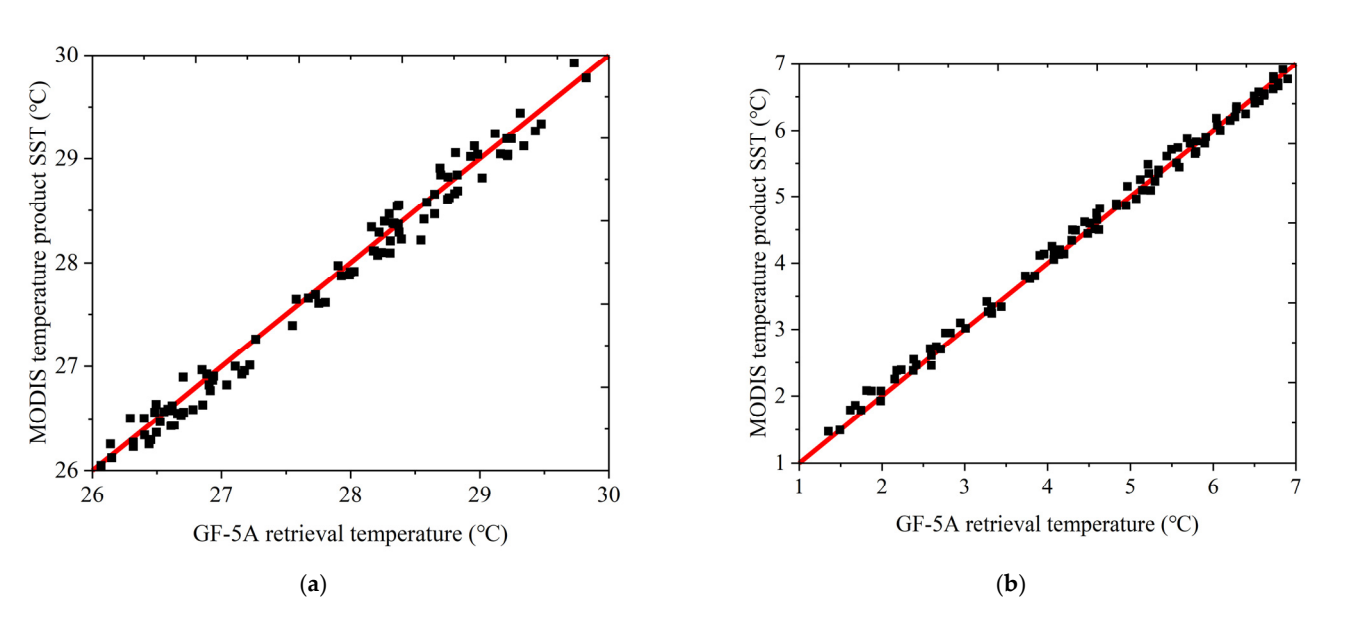


Figure 9. Indirect verification of the accuracy of SST retrieval from GF-5A images. (a) 18 July 2024; (b) 31 December 2024.

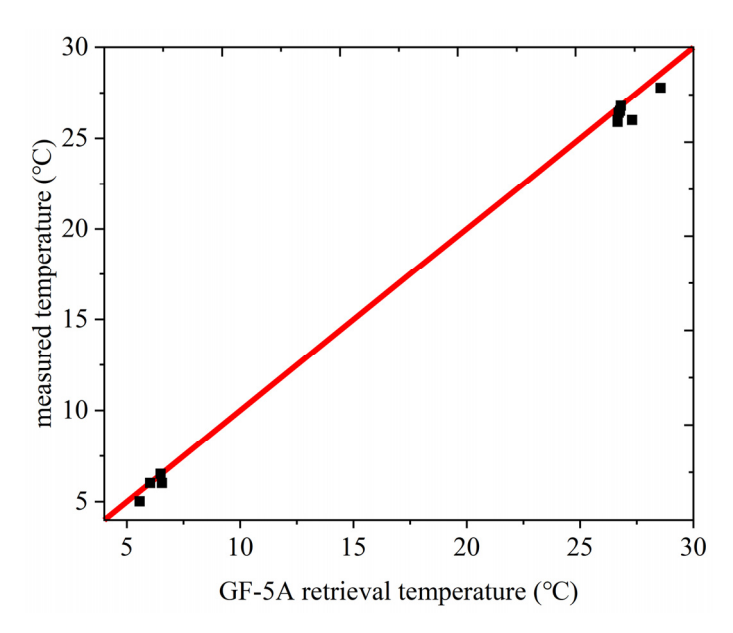


Figure 10. Direct verification of the accuracy of SST retrieval from GF-5A images.

The high-resolution Landsat 8 satellite temperature retrieval results have an R^2 of 0.923 and an *RMSE* of 0.385K compared to MODIS temperature product, and an R^2 of 0.984 and an *RMSE* of 0.742K compared to measured data [42,43].

This study indirectly verified the accuracy of retrieving SST from two GF-5A images using MODIS temperature product, with R^2 greater than 0.923 and RMSE less than 0.385 K. Compared with Landsat 8 data, the SST retrieval results of this study have better linear correlation and smaller comprehensive error with MODIS temperature product.

Due to the fact that the GF-5A satellite will not be officially put into use until 2024 and has a long observation period, this study used two GF-5A images representing summer and winter to achieve SST retrieval. This resulted in a limited number of measured data available for direct accuracy verification and their distribution being polarized. Therefore, although the accuracy of this study directly verifies that the R^2 in the results is as high as 0.999, it cannot explain the linear correlation between the measured data and the SST retrieval results of this study. However, the RMSE value is not affected by polarized measured data and is less than 0.742K, indicating that compared with Landsat 8 data, the comprehensive error between the SST retrieval results of this study and the measured data is smaller.

In summary, the SST retrieval results of this study have high direct and indirect validation accuracy.

5. Discussion

Although this research has facilitated the retrieval of SST data in Bohai Bay with high precision, it still has errors that affect the accuracy of SST retrieval.

- (1) The sea surface emissivity was 0.995, however, the actual specific sea surface emissivity value is affected by sediment content, wave conditions, and observation geometric conditions.
- (2) The atmospheric transmittance correction in this study was calculated using the effective wavelength, however, atmospheric transmittance correction using real-time atmospheric profile data is more accurate.
- (3) There is a difference between the depth of the SST of the measured data used in this study and that of the SST retrieved by the GF-5A satellite. The SST retrieved by the GF-5A satellite is the average temperature in a few microns-thick layer of the sea

Remote Sens. 2025, 17, 1879 14 of 16

surface, whereas the SST of the measured data is the temperature in the 0.1 m to 1 m deep layer of the sea surface. This difference leads to errors in the direct verification of SST retrieval accuracy.

(4) Wind, cloud, and other weather conditions also reduce SST retrieval accuracy. Cloud removal cannot completely eliminate the impact of clouds on SST retrieval accuracy. Therefore, to improve the accuracy of SST measurement in the Bohai Bay region further, it is necessary to collect and analyze data on the weather in this region.

6. Conclusions

The following conclusions can be drawn from this study:

- (1) An SST retrieval method based on the GF-5A satellite's Qin split window algorithm and parameter adjustment is proposed. This method utilizes GF-5A satellite data with a resolution of 100 m to obtain the effective wavelengths of various thermal infrared bands through spectral response functions. Then, two important parameters, atmospheric transmittance and regression coefficient, in the Qin split window algorithm are corrected to facilitate SST data retrieval in the Bohai Bay area, demonstrating the feasibility of this method.
- (2) Through image comparison, it has been proven that the spatial distribution of SST results retrieved from the Bohai Bay area using this method is similar to the MODIS temperature product SST data. In summer, SST gradually decreases from land to sea, while in winter, SST gradually increases from land to sea. Therefore, this method can be used to obtain large-scale real-time SST data, providing basic SST data for related research, such as studies of animal and plant resources.
- (3) Indirect verification using MODIS temperature product and direct verification using measured data have proven that the SST retrieval method has good accuracy in the Bohai Bay area, with better *R*² and *RMSE* values compared with the split window algorithm for SST retrieval of Landsat–8 satellite data at a resolution of 100 m. Therefore, this method can be used to obtain high-precision SST data that can be used for intelligent forecasting of ocean temperature and conducting other research studies.

Author Contributions: Conceptualization, J.S. and D.Z.; methodology, J.S. and D.Z.; validation, J.S., D.Z. and Z.S.; writing—original draft preparation, J.S. and D.Z.; writing—review and editing, D.W., D.Z and Z.S. All authors have read and agreed to the published version of the manuscript.

Funding: This research was funded by the Key Research and Development Program sponsored by the Ministry of Science and Technology (MOST) 2023YFC3107701, 2023YFC3107901 and the National Natural Science Foundation of China (No. 42375143), was also funded by Key Laboratory of Smart Earth, No. KF2023YB03-03.

Data Availability Statement: The data presented in this study are available on request from the corresponding author due to privacy restrictions.

Acknowledgments: The authors would like to acknowledge the anonymous reviewers for their valuable comments.

Conflicts of Interest: Author Zhiwei Sun was employed by the company Beijing Geoway Info-Tech Co., Ltd. The remaining authors declare that the research was conducted in the absence of any commercial or financial relationships that could be construed as a potential conflict of interest.

References

- Durán-Campos, E.; Coria-Monter, E. Early Signals of El Niño 2023 in the Gulf of California? Lat. Am. J. Aquat. Res. 2024, 52, 2024.
 [CrossRef]
- 2. Zhang, C.; Zhou, S.; Zhu, L. Three Algorithms of Sea Surface Temperature Inversion of Daya Bay Based on Environmental Star HJ_1B Data. *J. East China Univ. Technol. (Nat. Sci.)* **2013**, *36*, 88–92.

3. Zhang, C.; Zhang, X.; Zeng, Y.; Pan, W.; Hua, L. Retrieval and Validation of Sea Surface Temperature in the Taiwan Strait Using MODIS Data. *Acta Oceanol. Sin.* **2008**, *30*, 153–160.

- 4. Price, J.C. Estimating Surface Temperatures from Satellite Thermal Infrared Data—A Simple Formulation for the Atmospheric Effect. *Remote Sens. Environ.* **1983**, *13*, 353–361. [CrossRef]
- 5. Qin, Z.; Karnieli, A.; Berliner, P. A Mono-Window Algorithm for Retrieving Land Surface Temperature from Landsat TM Data and Its Application to the Israel-Egypt Border Region. *Int. J. Remote Sens.* **2010**, *22*, *3719–3746*. [CrossRef]
- 6. Qin, Z.-H.; Zhang, M.-H.; Karnieli, A.; Berliner, P. Mono-Window Algorithm for Retrieving Land Surface Temperature from Landsat TM6 Data. *Acta Geogr. Sin.* **2001**, *56*, 456–466.
- 7. Qin, Z.; Li, W.; Zhang, M.; Karnieli, A.; Berliner, P. Estimating of the Essential Atmospheric Parameters of Mono-Window Algorithm for Land Surface Temperature Retrieval from Landsat TM6. *Remote Sens. Land Resour.* **2003**, *15*, 37–43.
- 8. Jiménez-Muñoz, J.C.; Sobrino, J.A. A Generalized Single-Channel Method for Retrieving Land Surface Temperature from Remote Sensing Data. *J. Geophys. Res. Atmos.* **2003**, *108*, D22. [CrossRef]
- 9. Jimenez, J.-C.; Cristóbal Rosselló, J.; Sobrino, J.; Sòria Barres, G.; Ninyerola, M.; Pons, X. Revision of the Single-Channel Algorithm for Land Surface Temperature Retrieval from Landsat Thermal-Infrared Data. *Geosci. Remote Sens. IEEE Trans.* 2009, 47, 339–349. [CrossRef]
- 10. Jimenez, J.-C.; Sobrino, J.; Skokovic, D.; Mattar, C.; Cristóbal Rosselló, J. Land Surface Temperature Retrieval Methods from Landsat-8 Thermal Infrared Sensor Data. *Geosci. Remote Sens. Lett. IEEE* **2014**, *11*, 1840–1843. [CrossRef]
- 11. Gan, F.; Chen, W.; Zhang, X.; Yan, B.; Liu, S.; Yang, S. The Progress in the Study of Thermal Infrared Remote Sensing for Retrieving Land Surface Temperature. *Remote Sens. Land Resour.* **2006**, *18*, 6–11.
- 12. Ding, F.; Xu, H. Comparison of Three Algorithms for Retrieving Land Surface Temperature from Landsat TM Thermal Infrared Band. *J. Fujian Norm. Univ. Nat. Sci. Ed.* **2008**, 24, 91–96.
- 13. Li, H.; Zeng, Y.; Fu, P.; Huang, J.; Yang, K.; Zou, J. Study on Retrieval Urban Land Surface Temperature with Multi-source Remote Sensing Data. *Natl. Remote Sens. Bull.* **2007**, *11*, 891–898.
- 14. McMillin; Larry, M. Estimation of Sea Surface Temperatures from Two Infrared Window Measurements with Different Absorption. J. Geophys. Res. 1975, 80, 5113–5117. [CrossRef]
- 15. Zhu, L.; Gu, X.; Chen, L.; Yu, T.; Wang, Z.-F. Comparison of LST Retrieval Precision between Single-Channel and Split-Windows for High-Resolution Infrared Camera. *J. Infrared Millim. Waves* **2008**, *27*, 346–353.
- 16. Qin, Z.; Karnieli, A. Progress in the Remote Sensing of Land Surface Temperature and Ground Emissivity Using NOAA-AVHRR Data. *Int. J. Remote Sens.* **1999**, *20*, 2367–2393. [CrossRef]
- 17. Zhang, L.; Mei, G.; Liu, M.; Li, Y.; Shi, K.; Zhu, M.; Li, H.; Guo, Y.; Wang, J. Comparison of Lake Surface Water Temperature Retrieval Algorithms: A Case Study of Lake Qiandaohu. *Natl. Remote Sens. Bull.* **2024**, 28, 2113–2130. [CrossRef]
- 18. Qin, Z.; Zhang, M.; Karnieli, A. Split Window Algorithms for Retrieving Land Surface Temperature from Noaa-Avhrr Data. *Remote Sens. Land Resour.* **2001**, *13*, 33–42.
- 19. Sun, T.; Yang, K.; Wang, X.; Zhang, W.; Cheng, L. Study on the Suitability of Split-Window and Mono-Window Algorithms on Analying the Urban Heat Island Effect of Tai'an City. *Geomat. Spat. Inf. Technol.* **2017**, *40*, 60–63.
- 20. Wang, Y.; Song, X.; Tang, B.; Li, Z.; Leng, P. Validation of FY-2C Derived Land Surface Temperature over the Source Region of the Yellow River: A Case Study of Maqu County. *Remote Sens. Land Resour.* **2015**, 27, 68–72.
- 21. Pandya, M.; Shah, D.; Trivedi, H.; Panigrahy, S.; Parihar, J.; Kirankumar, A. Evaluation of Split-Window Algorithms for Retrieving Land Surface Temperature from the INSAT-3D Imager Observations. In *Vayumandal*; Indian Meteorological Society: New Delhi, India, 2011; pp. 35–41.
- 22. Jiang, G.-M.; Li, Z.-L. Split-Window Algorithm for Land Surface Temperature Estimation from MSG1-SEVIRI Data. *Int. J. Remote Sens.* **2008**, 29, 6067–6074. [CrossRef]
- 23. Gao, C.; Tang, B.; Wu, H.; Jiang, X.; Li, Z.-L. A Generalized Split-Window Algorithm for Land Surface Temperature Estimation from MSG-2/SEVIRI Data. *Int. J. Remote Sens.* **2013**, *34*, 4182–4199. [CrossRef]
- 24. Liu, C.; Li, H.; Du, Y.; Cao, B.; Liu, Q.; Meng, X.; Hu, Y. Practical Split-Window Algorithm for Retrieving Land Surface Temperature from Himawari 8 AHI Data. *Natl. Remote Sens. Bull.* **2021**, *21*, 702–714. [CrossRef]
- 25. Jiang, G.-M.; Zhou, W.; Liu, R. Development of Split-Window Algorithm for Land Surface Temperature Estimation from the VIRR/FY-3A Measurements. *IEEE Geosci. Remote Sens. Lett.* **2013**, *10*, 952–956. [CrossRef]
- 26. Yang, J.; Huang, C.; Mo, W.; Wu, Y.; Shen, J.; He, L.; Chen, S. Comparison and Application for Different Split Window Algorithm of Retrieving Land Surface Temperature. *J. Guangxi Univ.* (*Nat. Sci. Ed.*) **2004**, 29, 80–85.
- 27. Ding, L.; Qin, Z.; Mao, K. A Research of Split Window Algorithm Based on MODIS Image Data and Parameter Determination. *Remote Sens. Technol. Appl.* **2005**, 20, 284–289.
- 28. KANG, T.; GUO, M.; Cao, B.; Ren, H.; Fan, W. Component Temperature Inversion Algorithm Based on Sentinel-3 SLSTR Data. *Yaogan Xuebao/J. Remote Sens.* **2021**, 25, 1671–1682. [CrossRef]

29. Bai, Q.; Meng, D.; Xing, J. Study on Land Surface Temperature Retrieval in Beijing Based on Tiangong-2 Data. *Manned Spacefl.* **2019**, 25, 809–816.

- 30. Cheng, Y.; Wu, H.; Li, Z.; Qian, Y. Retrieval and Validation of the Land Surface Temperature from FY-3D MERSI-II. *Natl. Remote Sens. Bull.* **2021**, 25, 1792–1807. [CrossRef]
- 31. Fang, C.; Liang, X.; Liu, R. Comparative Analysis of Marine Economic Difference Based on Geospatial Gulfs: A Case Study of Liaodong Bay, Bohai Bay, Laizhou Bay. *China Popul. Resour. Environ.* **2012**, 22, 170–174.
- 32. Yang, L.; Liu, J.; Zhang, J.; Wang, X.; Xu, Y.; Li, X.; He, L. Zooplankton Community Variation and Its Relationship with Environmental Variables in Bohai Bay. *J. Mar. Sci.* **2018**, *36*, 93–101.
- 33. Zheng, X.; Li, G. Distribution Characteristics of Chlorophyll Concentration and the Effects of Environmental Elements of Bohai Bay in Spring. *Ocean Technol.* **2014**, *33*, 1–7.
- 34. Zhang, Y.; Gu, D.; Xu, H.; Xue, W.; Yu, X. Environmental Adaptability of Fish Eggs in Bohai Bay Assessed Using Habitat Suitability Index Method. *J. Fish. Sci. China* **2021**, *28*, 1568–1575. [CrossRef]
- 35. Bao, X. Simulation of Seasonal Variation of Thermo-Structure and Circulation in the Bohai and Yellow Seas. *Period. Ocean. Univ. China* **2004**, *34*, 513–522.
- 36. Tian, M.; Tian, Z.; Feng, Q.; Fan, Y.; Dong, N.; Shao, Y.; Wang, Z. Monthly Average Variation Pattern of Key Ecological and Environmental Parameters in Bohai Bay over the Past Two Decades. *Adv. Geosci.* **2024**, *14*, 1247–1255. [CrossRef]
- 37. Mao, K.; Qin, Z.; Wang, J.; Wu, S. Lowtran Retrieval of Atmospheric Water Content and Transmittance Computation of MODIS Bands 31 and 32. *Remote Sens. Land Resour.* **2005**, *17*, 26–29.
- 38. Wang, T.; Song, M.; Hou, Q. Research on Surface Temperature Inversion and Its Application in Chongqing Based on Split Window Algorithm. *Mod. Inf. Technol.* **2024**, *8*, 93–98.
- 39. Mao, K.; Tang, H.; Zhou, Q.; Chen, Z.; Chen, Y.; Qin, Z. Retrieving land surface temperature from MODIS data by using radiance transfer equation. *J. Lanzhou Univ.* (*Nat. Sci.*) **2007**, *43*, 12–17.
- 40. Gao, M.; Qin, Z.; Xu, B. Estimation of the Basic Parameters for Deriving Surface Temperature from MODIS Data. *Arid Zone Res.* **2007**, 24, 113–119.
- 41. Hang, Y.; Zhang, P. Retrieval of Lake Surface Temperature in Plateau Based on Landsat-8 Images. J. Appl. Sci. 2024, 42, 977–987.
- 42. Zhai, S.; Huang, D.; Wang, W.; Liu, J.; Wang, H.; Lu, Z. Land Surface Temperature Retrieval Using Improved Splitting Window Algorithm Based on Landsat 8 Data. *J. China Hydrol.* **2019**, *39*, 8–13.
- 43. He, G.; Hu, Y.; Xiao, Z. Land Surface Temperature Retrieval Based on TM8 Thermal Infrared Data and Its Application. *Guangdong Agric. Sci.* **2015**, 42, 146–153.

Disclaimer/Publisher's Note: The statements, opinions and data contained in all publications are solely those of the individual author(s) and contributor(s) and not of MDPI and/or the editor(s). MDPI and/or the editor(s) disclaim responsibility for any injury to people or property resulting from any ideas, methods, instructions or products referred to in the content.